Salt-Driven Dynamic Regulation of Permeability in Dispersive Soil: A Macroscopic and Microscopic Investigation

Junting Liu*
Key Laboratory of Urban Security and Disaster Engineering of Ministry of Education, Beijing University of Technology, Beijing, China
**Corresponding author*

Abstract: Dispersive soil is a special type of soil widely distributed around the world, and its susceptibility to erosion upon contact with low-salinity water poses significant challenges to hydraulic engineering. The understanding of its seepage characteristics, particularly the role of salt in regulating permeability, remains limited. In this study, typical dispersive soils from Da'an City were collected, and remolded specimens with varying salt contents (0%, 0.3%, 1.0%, 1.5%, and 2.0%) were prepared. Variable-head saturated permeability tests were conducted in conjunction with scanning electron microscopy (SEM) observations to investigate the time-dependent permeability behavior and the underlying microstructural mechanisms. The results show that the permeability coefficient of dispersive soil exhibits a decreasing trend over time, with the attenuation concentrated in the initial stage of seepage. Salt content is positively correlated with the initial permeability coefficient, with the high-salt group showing a considerably higher initial permeability than the salt-free group. However, this enhancing effect diminishes significantly with seepage duration, and the difference between groups narrows substantially by the second day. SEM observations reveal that medium-salt conditions (1.0%–1.5%) facilitate the formation of a stable flocculated structure that maintains favorable permeability, whereas high-salt conditions (2.0%) produce a loose flocculated structure that undergoes degradation upon salt leaching, leading to a rapid decline in permeability. The findings demonstrate that salt dynamically regulates the permeability of dispersive soil by controlling microstructural evolution, providing a theoretical basis for the long-term performance assessment of saline dispersive soil under engineering seepage conditions.

Keywords: Dispersive Soil; Salt Content; Permeability Coefficient; Microstructural Evolution; Seepage Characteristics

1. Introduction

Dispersive soil is a special type of soil widely distributed around the world and has gradually become a key focus in the field of hydraulic engineering over the past two decades. In the Songnen Plain of China, locally prevalent dispersive soil frequently leads to issues such as slope instability and channel collapse [1]. Its distinct characteristic lies in the rapid loss of most of its internal cohesion upon contact with low-salinity water, causing the soil particles to disintegrate into primary particles. Clay particles remain suspended in water in colloidal form, making aggregation difficult, and the soil structure rapidly deteriorates due to the loss of cementing materials [2-5]. To date, most research on dispersive soil has focused on engineering improvements using chemical or biological additives [6], such as promoting the aggregation of soil particles through mechanisms like electrostatic attraction, flocculation, and agglomeration to achieve stabilization. Yuan et al. [7] successfully reduced soil dispersivity by utilizing microbial urease to catalyze the formation of calcium carbonate, which binds soil particles. Xu et al. [8]employed nano-silica sol to fill soil pores, generating calcium silicate hydrate (CS-H). However, the effectiveness of these chemical methods typically diminishes over time, exhibiting poor long-term stability [9]. Moreover, dispersivity only manifests upon interaction with water, and current understanding of its hydraulic properties remains limited.

Dispersive soil primarily damages natural landscapes or engineering structures through erosion [10-16]and is more susceptible to internal erosion under the influence of seepage [17].

 Copyright @ STEMM Institute Press

Although the consequences of erosion caused by seepage are readily identifiable, the characteristics of water movement within soil pores remain poorly understood and warrant systematic investigation. Numerous engineering failures are induced by seepage processes, such as erosion [18-19], fracturing [20], shallow landslides [21], and dam deformation [22-23]. Given the relatively limited research on seepage in dispersive soils, studies on other soil types can provide valuable insights. For instance, Lin et al. [24] conducted long-term seepage tests on loess and found that soluble salts redistributed with water migration, subsequently inducing structural changes. She et al. [25] confirmed that divalent cations in expansive soils migrate downward under unidirectional seepage conditions. Qin et al. [26] proposed that the seepage process in loess under single-point water supply can be divided into rapid and stable stages.

Changes in soil salinity can also influence the seepage field by altering soil structure, making it essential to consider the role of salt when investigating the seepage characteristics of dispersive soil. Existing studies indicate that the scaling mechanism of unsaturated dispersive soil in cold and arid regions is closely related to soil salinity, and that salt plays a crucial role in controlling seepage velocity [27-28]. However, the transport processes of water and soluble salts within the soil are highly complex [29], and the patterns of soluble salt migration with water flow in dispersive soil remain to be thoroughly explored. Although some studies have examined the effect of salt on the soil-water characteristic curve, noting that an increase in sodium bicarbonate content reduces matric suction [28], the relationship between salt and soil-water properties remains unclear. Some research suggests a positive correlation or suction dependence [30-33], while others have found no significant correlation [34-36]. Additionally, factors such as dry density further complicate the prediction of soil-water characteristics [37-40].

Against this backdrop, this study selects typical dispersive soil from the western region of Jilin Province. By preparing remolded specimens with varying salt contents and conducting variable-head saturated permeability tests combined with microscopic observations using scanning electron microscopy, this study aims to:

(1) elucidate the time-dependent behavior of dispersive soil under seepage conditions;

(2) analyze the mechanisms by which salt content influences pore structure and seepage characteristics;

(3) reveal the micro-level mechanisms governing the effect of salt content on the permeability of dispersive soil.

2. Materials and Methods

2.1 Materials

The Soils for this study were collected from the western part of Da'an City, Jilin Province, China. According to the standard laboratory tests of the U.S. Soil Conservation Service, both Soil A and Soil B were classified as dispersive soils. In the crumb test, both samples reacted vigorously with water, with colloidal deposits rapidly forming at the bottom of the beaker and causing turbidity throughout the water. In the pinhole test, under a head of 50 mm, the flow rates for the two Soils were 1.95 mL/s (Soil A) and 1.65 mL/s (Soil B), respectively, and after the test, the pinhole diameter exceeded 1.5 times its initial size. The dispersivity values measured by the double hydrometer test were 93.5% and 92.4%, respectively. The particle size distribution of both soils was dominated by clay: the sand, silt, and clay contents were 11.9% and 12.9%, 23.3% and 25.4%, and 64.8% and 61.7% for Soil A and Soil B, respectively. The initial salt contents of the two Soils were 11.3 g/kg (Soil A) and 22.8 g/kg (Soil B), with Na^+ and HCO_3^- being the predominant cation and anion, respectively.

Table 1 presents the soluble salt content results and basic physical property indices for the two Soils: Soil A had a particle density of 2.64 g/cm^3, a liquid limit of 38.6%, and a plastic limit of 19.2%; Soil B had a particle density of 2.65 g/cm^3, a liquid limit of 40.6%, and a plastic limit of 13.2%. The compaction characteristics of the two Soils differed: Soil A exhibited a maximum dry density of 1.64 g/cm^3 and an optimum moisture content of 14.4%; Soil B exhibited a maximum dry density of 1.74 g/cm^3 and an optimum moisture content of 11.9%. The mineral composition, determined by X-ray diffraction (according to SY/T 5163-2018), is presented in Table 2. The results show that quartz was the most abundant mineral (48.4% in Soil A and 52.9% in Soil B), followed by plagioclase (24.2% in Soil A and 13.5% in Soil B) and calcite (11.6% in Soil A and 15.5% in Soil B). Regarding total clay mineral content,

Copyright @ STEMM Institute Press

Soil A contained 5.0% and Soil B contained 3.4%. Notably, the clay mineral compositions differed significantly between the two samples: Soil A was dominated by illite (41%) and illite/smectite mixed-layer (32%), whereas Soil B mainly contained illite (64%) along with a relatively higher kaolinite content (21%).

2.2 Preparation of Samples

When preparing remolded dispersive soil specimens, conventional salt-washing treatment was not employed in order to preserve the natural dispersive characteristics of the soil. Conventional salt-washing typically involves mixing the Soil with sufficient distilled water to form a soil-water mixture, allowing soluble salts to fully dissolve. The soil particles and salt solution are then separated through centrifugation, filtration, or static settling followed by decanting of the supernatant. This washing process usually needs to be repeated multiple times until the electrical conductivity of the washing solution stabilizes or reaches a very low value, indicating that soluble salts have been largely removed. However, during practical application, it was observed that extremely fine particles were dispersed and remained suspended in the supernatant throughout the salt-washing process. Considering the impracticality of this process and the fact that immersion of the soil leads to colloidal dispersion of fine particles, thereby distorting the particle size distribution, this study directly used air-dried soil sieved through a 2 mm mesh for specimen preparation, so as to preserve the original dispersive potential of the soil to the greatest extent possible. The salt content c of the saline soil in this paper is defined as follows:

$$c=\frac{m_{salt}}{m_s+m_{salt}} \quad (1)$$

In the formula, m_s represents the mass of soil particles, and m_{salt} represents the mass of salt. The compaction method was employed to control the target dry density of the remolded soil specimens at 1.4 g/cm^3. Specimens were prepared using standard compaction rings with an inner diameter of 61.8 mm and a height of 40 mm. The salt content c was set to 0%, 0.3%, 1%, 1.5%, and 2%, respectively.

2.3 Penetration Test Plan

The variable-head method was employed to determine the permeability coefficient of the dispersive soil. Prior to permeability testing, the soil specimens were saturated using a vacuum saturation device, with the saturation fluid being salt solutions corresponding to each salt content level (see Fig.1). During permeability testing, distilled water was used as the permeating fluid, as dispersive soil exhibits adverse dispersive characteristics when eroded by water, particularly upon contact with pure water; therefore, distilled water was used to simulate rainfall infiltration. The valves of the inlet and outlet tubes were kept open, and the initial and final water head heights in the piezometric tube were recorded at regular intervals to calculate the permeability coefficient accordingly. Subsequently, the water head height was adjusted, and the above measurements were repeated. Each set of tests lasted no less than six days to monitor the time-dependent variation of the permeability coefficient of the dispersive soil.

2.4 Scanning Electron Microscope Test

To analyze the changes in the microscopic pore structure characteristics of dispersive soil in the Da'an region after permeation, this study employed scanning electron microscope (SEM) tests to obtain the microstructure characteristics of the Soils. Microscopic images were captured using the scanning electron microscope, and the resulting images were digitally processed and analyzed. For each salt concentration level, two sets of specimens were prepared under identical conditions and saturated simultaneously. One set was reserved as a control after saturation, while the other set was subjected to permeability tests. Both the control specimens and the post-permeation specimens were prepared into samples with cross-sectional dimensions of 1 cm × 1 cm and a length of 3.5 cm, and then freeze-dried to meet the testing requirements。

3. Results and Discussion

3.1 Permeability Aging Characteristics

The permeability test results indicate that, under all salt concentration levels, both types of dispersive soil exhibited a common trend of decreasing permeability coefficients over time, with the attenuation process primarily occurring in the early stages of the test. As shown in Figure 2, within the first day after the initiation of permeation, the permeability coefficient decreased most significantly; starting from the second day, the rate of decline notably narrowed,

 Copyright @ STEMM Institute Press

and the curves gradually flattened. Taking Soil A as an example, in the 2.0% salt content group, the permeability coefficient decreased from 120×10^{-7} to approximately 70×10^{-7}cm/s，within the first day, declining by more than 40%. From the second day until the end of the test, the decrease was less than 10×10^{-7}cm/s. Soil B exhibited a similar evolution pattern.。

3.2 The Effect of Salt on the Permeability Coefficient

There is a clear positive correlation between salt content and the permeability coefficient. At the first measurement time (T_1), the permeability coefficient showed a pronounced increasing trend with higher salt content. Taking Soil A as an example, the initial permeability coefficient of the 0% salt content group was approximately 40×10^{-7} cm/s, whereas that of the 2.0% salt content group reached about 100×10^{-7}cm/s， representing an increase of approximately 60×10^{-7}cm/s 。 For Soil B, the increase in the initial permeability coefficient of the high-salt group compared to the salt-free group was of a similar magnitude (see Fig. 3 and 4).

However, the enhancing effect of salt on the permeability coefficient exhibited significant temporal attenuation. Comparing the curves at the first moment (T_1) of the first day with those at the last moment (T_7), the intervals between curves corresponding to different salt contents were notably reduced. By the second day, the permeability coefficient curves at different times within a single day had nearly converged, and the difference between the high-salt group and the salt-free group had diminished to less than 10×10^{-7}cm/s. Within a given day, the permeability coefficient curves occasionally exhibited brief fluctuations or slight increases, which were primarily attributed to operational factors such as water head resetting and system equilibrium inherent in the variable-head test method, and did not affect the overall trend.

3.3 SEM Microstructure Observation Results

To elucidate the mechanisms underlying the macroscopic permeability behavior from a microscopic perspective, this study employed scanning electron microscopy to conduct comparative observations of Soils that had undergone saturation and the complete permeation process. The observation results are systematically arranged by salt concentration gradient, with images on the left showing the initial state after saturation but prior to permeation, and images on the right showing the final state after the permeation tests (see Fig. 5 and 6).

For salt-free (0%) and low-salt (0.3%) Soils, the pre-permeation microstructure exhibited a state of particle dispersion or incipient flocculation, with a relatively dense pore system. After permeation, the microscopic images of these Soils generally showed signs of fine particle migration, localized pore clogging, or structural compaction. For medium-salt (1.0%, 1.5%) Soils, a typical and stable flocculated structure was observed after saturation, with clay particles forming robust aggregates that constituted a well-connected pore network. Following permeation, the microstructure demonstrated a high degree of stability, with the flocculated framework and pore morphology being well preserved. For high-salt (2.0%) Soils, the structure was most open and loose after saturation, with numerous macropores developing between flocculated aggregates. However, images taken after permeation revealed significant degradation of this open structure, manifested as partial collapse of the flocculated aggregates, a reduction in macropores, and the presence of voids or deposits potentially left by the dissolution of salt crystals.

4. Disscussion

4.1 Analysis of Penetration Test Result

The macroscopic permeability behavior described above reveals the dynamic regulatory mechanism of salt on the permeability characteristics of dispersive soil. The rapid decrease in the permeability coefficient during the initial stage indicates that the internal pore structure of the soil undergoes a period of rapid adjustment at the onset of seepage, followed by a relatively slow evolution phase. This phenomenon is closely related to the high sensitivity of dispersive soil to water: under the action of freshwater seepage, the original chemical equilibrium within the soil is disrupted, and the inter-particle bonding modes adjust, leading to a gradual stabilization of the pore structure.

The positive correlation between salt content and the initial permeability coefficient can be explained by the electric double layer theory.

Copyright @ STEMM Institute Press

Under high-salt conditions, the higher ion concentration in the pore fluid compresses the thickness of the electric double layer around the particles, reduces electrostatic repulsion between particles, and promotes flocculation of clay particles, forming a relatively open flocculated structure that provides favorable seepage pathways at the initial stage. This mechanism accounts for why the high-salt groups exhibited higher permeability coefficients at the beginning of the test.

It is noteworthy that the enhancing effect of salt on permeability diminishes significantly with seepage duration. This behavior of "high initial value, rapid attenuation" suggests that the microstructures formed under different salt concentrations differ fundamentally in their stability. Although the open pore network formed under high-salt conditions provides excellent seepage pathways initially, its stability is highly dependent on the high-salt environment of the pore fluid. As freshwater seepage continues, the salt within the soil is gradually leached out, leading to increased electrostatic repulsion between particles, degradation of the original flocculated structure, a reduction in seepage channels, and a consequent decrease in macroscopic permeability. This phenomenon was consistently observed in both Soils, indicating the universality of this mechanism.

4.2 Discussion on the Mechanism of Microstructural Changes

The scanning electron microscopy observations corroborate the macroscopic permeability data, revealing the underlying mechanism by which salt regulates permeability from a microscopic perspective. Before permeation, the salt-free and low-salt Soils exhibited a dispersed or incipiently flocculated state with fine pores, corresponding to their low initial permeability coefficients macroscopically. The migration of fine particles and pore clogging observed after permeation provide a microscopic explanation for the trend of a continuously slow decline in the permeability coefficient of such Soils over time-namely, a sustained process of physical suffusion and structural adjustment. The stable flocculated structure formed in the medium-salt Soils serves as the microscopic foundation for their relatively high initial permeability coefficients and rapid attainment of a stable plateau. This structure effectively resists the physicochemical disturbances induced by freshwater seepage, thereby maintaining favorable seepage pathways. The microstructural evolution of the high-salt Soils elucidates the underlying cause of the macroscopically observed "high initial value, rapid attenuation" behavior. After saturation, their structure was the most open and loose, providing the highest initial permeability coefficient. However, the significant structural degradation following permeation directly accounts for the greatest decrease in permeability coefficient observed within the first day for this group. The fundamental mechanism lies in the fact that maintaining such an open flocculated system requires a high-ionic-strength pore fluid environment. Under continuous freshwater seepage, $NaHCO_3$ is progressively leached out, leading to an increased thickness of the electric double layer around the particles and greater electrostatic repulsion, while the "salt-bridge" bonding effect weakens, causing the flocculated structure to collapse and densify.

Synthesizing the macroscopic and microscopic analyses, salt compresses the electric double layer and promotes flocculation, thereby constructing the microstructural "skeleton" that governs permeability during the initial stage; the higher the salt content, the more open the skeleton and the greater the initial permeability. However, during long-term seepage, the durability of this skeleton depends on its inherent stability and the maintenance of the chemical environment. The medium-salt condition (approximately 1.0%–1.5%) achieves the optimal balance between these factors, forming a "stable flocculated" structure that yields the most stable permeability. In contrast, the "loose flocculated" structure formed under the high-salt condition (2.0%), despite offering exceptionally high initial water conductivity, exhibits stability highly dependent on environmental salts; upon salt leaching, it rapidly degrades, leading to a sharp decline in permeability performance.

5. Conclusions

(1) The permeability coefficient exhibits an overall decreasing trend over time, with the attenuation mainly concentrated in the early stage of the test, indicating that the internal structure of the soil undergoes rapid adjustment during the initial seepage phase and subsequently enters a relatively stable stage.

(2) Salt content is positively correlated with the

 Copyright @ STEMM Institute Press

initial permeability coefficient; the higher the salt content, the stronger the initial permeability. Taking the first-day data as an example, the initial permeability coefficient of the high-salt group was approximately 60×10^{-7}cm/s higher than that of the salt-free group. However, the loose flocculated structure formed under high-salt conditions exhibits poor stability, and this effect significantly diminishes with seepage duration. By the second day, the difference in permeability coefficient between different salt content groups had narrowed to less than 10×10^{-7}cm/s。

(3) Microstructural analysis reveals the dynamic mechanism underlying the influence of salt: medium-salt conditions (1.0%–1.5%) facilitate the formation of a stable flocculated structure, resulting in relatively stable permeability; whereas the loose flocculated structure formed under high-salt conditions (2.0%) is prone to degradation after salt leaching, leading to a rapid decline in permeability. This study elucidates the dynamic mechanism by which salt influences permeability through controlling microstructural evolution, providing a theoretical basis for the long-term performance assessment of saline dispersive soil under engineering seepage conditions.

References

[1] Xu, X., Li, J., Wang, Q., Chu, H., Lei, H., Wang, X., Meng, L., Ruan, Z., Du, H., 2025. Investigation into the mechanical properties and microscopic mechanisms of dispersive saline soil improved by environmentally friendly biopolymers. J. Environ. Chem. Eng. 13 (1), 115222.

[2] Bell, F.G., Walker, D.J.H., 2000. A further examination of the nature of dispersive soils in Natal, South Africa. Q. J. Eng. Geol. Hydrogeol. 33, 187–199.

[3] Fan, H., Kong, L., 2013. Empirical equation for evaluating the dispersivity of cohesive soil. Can. Geotech. J. 50 (9), 989–994.

[4] Quiñonez Samaniego, R.A., et al., 2021. Key parameters controlling strength and resilient modulus of a stabilised dispersive soil. Road Mater. Pavement Des. 1–16.

[5] Zorluer, I., Icaga, Y., Yurtcu, S., Tosun, H., 2010. Application of a fuzzy rule-based method for the determination of clay dispersibility. Geoderma 160 (2), 189–196.

[6] Zhou, Y.X., Yuan, X.Q., Wang, Q., Chen, H., Xu, X., 2026. A new strategy for improving the anti-dispersal properties and mechanical performance of dispersed soil in seasonal frozen regions: Research on the application of soybean urease-induced carbonate precipitation (SICP), Cold Reg. Sci. Technol. 246, 104882.

[7] Yuan, X., Wu, Y., Niu, C., Yang, X., L, Sen., Wu, Z., Wang, Q., Chen, H., Xu, X., Du, H.,2026. Durability analysis of using MICP to address dispersive soil issues in seasonal freezing areas. Soil Tillage Res. 257, 106924.

[8] Xu, X., Wang, X., Wang, Q., Yang, X., Meng, L., Lei, H., Yuan, X., Jin, C., 2026. Physicochemical, microstructure, mechanical properties, and mechanism of dispersive saline soil treated with nano-silica sol. Soil Tillage Res. 255, 106767.

[9] Xu, X., Lei, H., Wang, Q., Yuan, X., Guo, L., Yu, Z., 2024. Polyaluminum chloride (PAC) modification of dispersive soil: a comprehensive study on dispersivity, mechanical properties, and microscale mechanisms. Constr. Build. Mater. 425, 135890.

[10] Fell, R., Wan, C.F., Cyganiewicz, J., Foster, M., 2003. Time for development of internal erosion and piping in embankment dams. J. Geotech. Geoenviron. Eng. 129 (4), 307–314.

[11] García-Ruiz, J., Lasanta, T., Alberto, F., 1997. Soil erosion by piping in irrigated fields. Geomorphology 20 (3), 269–278.

[12] Han, M., et al., 2022a. Description of different cracking processes affecting dispersive saline soil slopes subjected to the effects of frost and consequences for the stability of low slopes. Bull. Eng. Geol. Environ. 81 (2), 75.

[13] Masoodi, A., Majdzadeh Tabatabai, M.R., Noorzad, A., Samadi, A., 2019. Riverbank stability under the influence of soil dispersion phenomenon. J. Hydrol. Eng. 24 (3), 05019001.

[14] Premkumar, S., Piratheepan, J., Arulrajah, A., Disfani, M.M., Rajeev, P., 2016. Experimental study on contact erosion failure in pavement embankment with dispersive clay. J. Mater. Civ. Eng. 28 (4), 04015179.

[15] Rui, X., Nie, L., Xu, Y., Wang, H., 2019. Land degeneration due to water infiltration and sub-erosion: A case study of soil slope failure at the National Geological Park of

Copyright @ STEMM Institute Press

Qianan Mud Forest, China. Sustainability 11 (17), 4709.

[16] Wang, L., Song, X., 2022. Engineering geological characteristics and failures of dispersive clays in Northeast China. Bull. Eng. Geol. Environ. 81 (3), 88.

[17] Vakili, A.H., Shojaei, S.I., Salimi, M., Selamat, M.R.B., Farhadi, M.S., 2020. Contact erosional behaviour of foundation of pavement embankment constructed with nanosilica-treated dispersive soils. Soils Found. 60 (1), 167–178.

[18] Chu-Agor, M.L., Fox, G.A., Cancienne, R.M., Wilson, G.V., 2008. Seepage caused tension failures and erosion undercutting of hillslopes. J. Hydrol. 359 (3–4), 247–259.

[19] Owoputi, L.O., Stolte, W.J., 2001. The role of seepage in erodibility. Hydrol. Process. 15 (1), 13–22.

[20] Richards, K.S., Reddy, K.R., 2012. Experimental investigation of initiation of backward erosion piping in soils. Geotechnique 62 (10), 933–942.

[21] Kim, M.S., Onda, Y., Uchida, T., Kim, J.K., Song, Y.S., 2018. Effect of seepage on shallow landslides in consideration of changes in topography: Case study including an experimental sandy slope with artificial rainfall. Catena 161, 50–62.

[22] Jiang, X., et al., 2020. Natural dam failure in slope failure mode triggered by seepage. Geomatics Natural Hazards & Risk 11 (1), 698–723.

[23] Li, X.S., Ming, H.Y., 2004. Seepage driving effect on deformations of San Fernando dams. Soil Dyn. Earthquake Eng. 24 (12), 979–992.

[24] Lin, G., Chen, W., Liu, P., Liu, W., 2019. Experimental study of water and salt migration in unsaturated loess. Hydrogeol. J. 27 (1), 171–182.

[25] She, J., Lu, Z., Yao, H., Fang, R., Xian, S., 2019. Experimental study on the swelling behavior of expansive soil at different depths under unidirectional seepage. Appl. Sci. 9 (6).

[26] Qin, Y., et al., 2022. Seepage characteristics in loess strata subjected to single point water supply. J. Hydrol. 609, 127611.

[27] Han, Y., et al., 2022b. Pore-scale study on the characteristic hydraulic conductivity of a dispersive lean clay affected by salinity and freeze–thaw. Bull. Eng. Geol. Environ. 81 (3), 107.

[28] Han, Y., et al., 2020. Experimental study on the hydraulic conductivity of unsaturated dispersive soil with different salinities subjected to freeze-thaw. J. Hydrol. 583, 124297.

[29] Zhang, X., Wu, Y., Zhai, E., Ye, P., 2021b. Coupling analysis of the heat-water dynamics and frozen depth in a seasonally frozen zone. J. Hydrol. 593, 125603.

[30] Fattah M. Y., Yahya A. Y., Al-Hadidi M.T., Ahmed B.A., 2013. Effect of salt content on total and matric suction of unsaturated soils. Eur. Sci. J. 9(9), 228–245.

[31] He Y., Zhang K., Wu D., 2019. Experimental and modeling study of soil water retention curves of compacted bentonite considering salt solution effects. Geofluids 4508603.

[32] Qin B., Lu Y., Chen Z., 2019. Chemical influence on water retention behaviour of compacted bentonite. Jpn. Geotech. Soc. Spec. Publ. 7(2), 174–178.

[33] Tang S., She D., Wang H., 2021. Effect of salinity on soil structure and soil hydraulic characteristics. Can. J. Soil. Sci. 101(1), 62–73.

[34] Ma T., Wei C., Chen P., Xia X., 2015. An experimental study of effect of NaCl solution on soil water characteristics. Rock Soil. Mech. 36(10), 2831–2836.

[35] Wang Y., Zhang A., Ren W., Niu L., 2019. Study on the soil water characteristic curve and its fitting model of Ili loess with high level of soluble salts. J. Hydrol. 578, 124067.

[36] Ying Z., Cui Y., Benahmed N., Duc M., 2021. Salinity effect on the compaction behaviour, matric suction, stiffness and microstructure of a silty soil. J. Rock Mech. Geotech. Eng. 13(4), 855–863.

[37] Birle E., Heyer D., Vogt N., 2008. Influence of the initial water content and dry density on the soil-water retention curve and the shrinkage behavior of a compacted clay. Acta Geotech 3(3), 191.

[38] Gallage C.P.K., Uchimura T., 2010 Effects of dry density and grain size distribution on soil-water characteristic curves of sandy soils. Soils Found 50(1), 161–172.

[39] Jacinto A.C., Villar M.V., Gomez-Espina R., Ledesma A., 2009. Adaptation of the van Genuchten expression to the effects of temperature and density for compacted bentonites. Appl. Clay Sci. 42(3–4),

 Copyright @ STEMM Institute Press

575–582.
[40] Jiang Y., Chen W., Wang G., Sun G., Zhang F., 2017 Influence of initial dry density and water content on the soil-water characteristic curve and suction stress of a reconstituted loess soil. Bull Eng. Geol. Environ 76(3), 1085–1095.

List of Figure captions

Figure 1– Penetration test process diagram

Figure 2 – Time-dependent characteristics of permeability coefficient in dispersive soils under different salinity levels

Figure 3 – Relationship between permeability coefficient and salinity for Soil A: a comparison across different measurement days

Figure 4 – Relationship between permeability coefficient and salinity for Soil B: a comparison across different measurement days.

Figure 5 – SEM images of Soil A before and after permeation. (a, f) distilled water; (b, g) 0.3% $NaHCO_3$; (c, h) 1.0% $NaHCO_3$; (d, i) 1.5% $NaHCO_3$; (e, j) 2.0% $NaHCO_3$.

Figure 6 – SEM images of Soil B before and after permeation. (a, f) distilled water; (b, g) 0.3% $NaHCO_3$; (c, h) 1.0% $NaHCO_3$; (d, i) 1.5% $NaHCO_3$; (e, j) 2.0% $NaHCO_3$.

Figure 1. Penetration Test Process Diagram

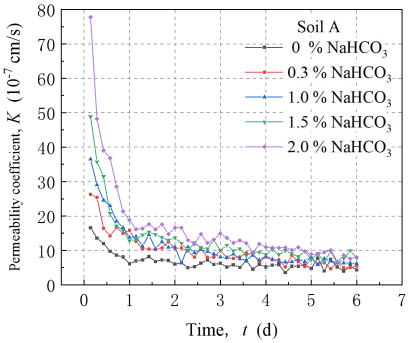

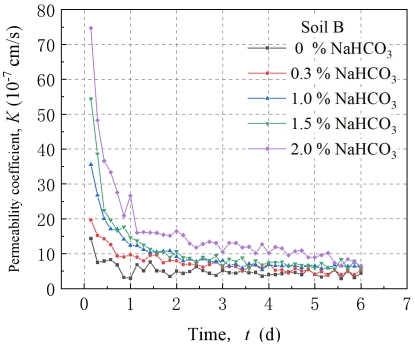

Figure 2. Time-dependent Characteristics of Permeability Coefficient in Dispersive Soils Under Different Salinity Levels

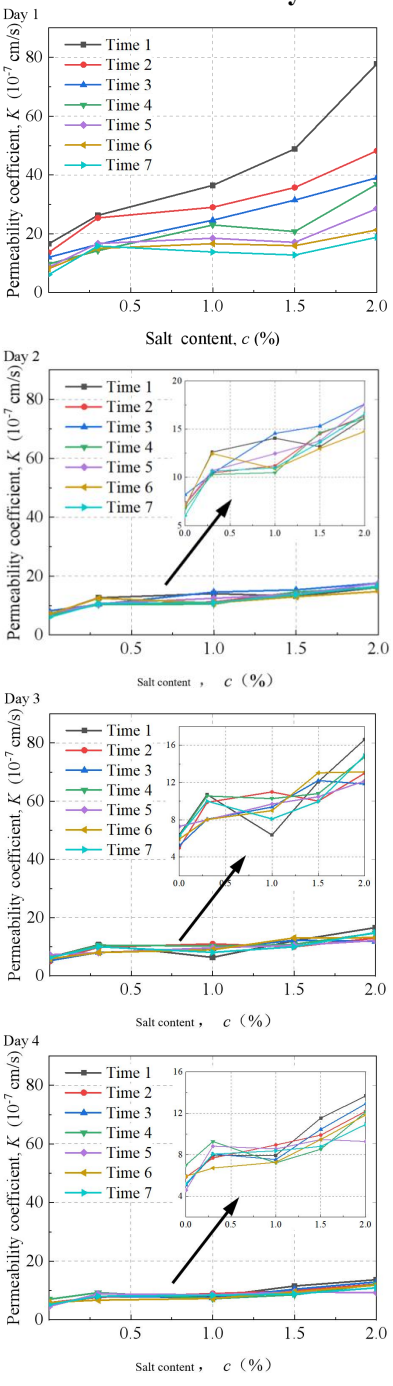

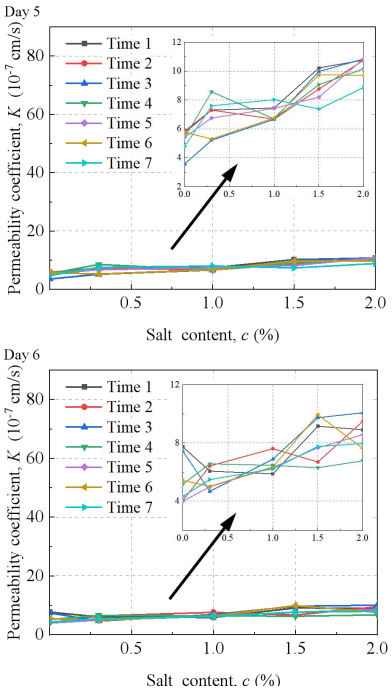

Figure 3. Relationship between Permeability Coefficient and Salinity for Soil A: a Comparison Across Different Measurement Days

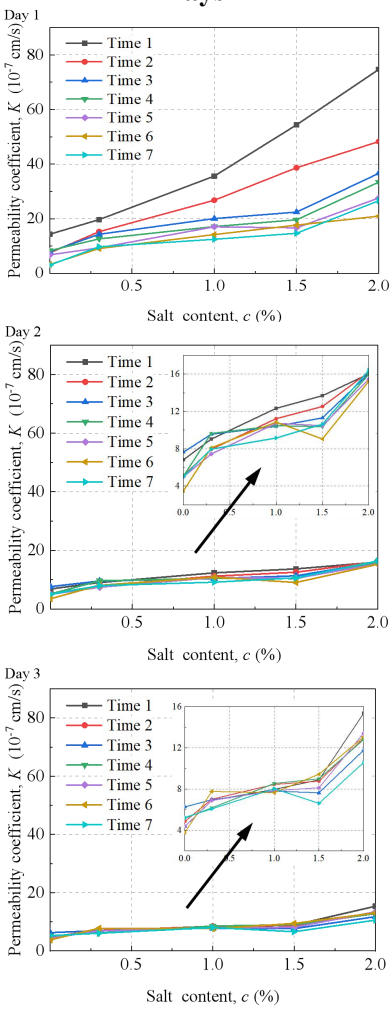

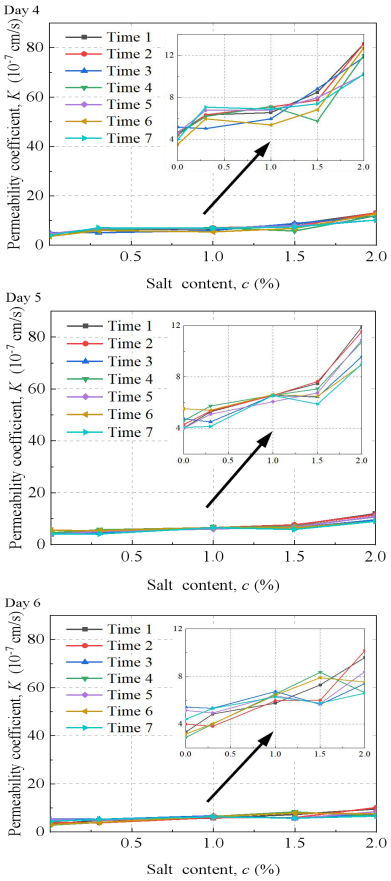

Figure 4. Relationship between Permeability Coefficient and Salinity for Soil B: a Comparison Across Different Measurement Days

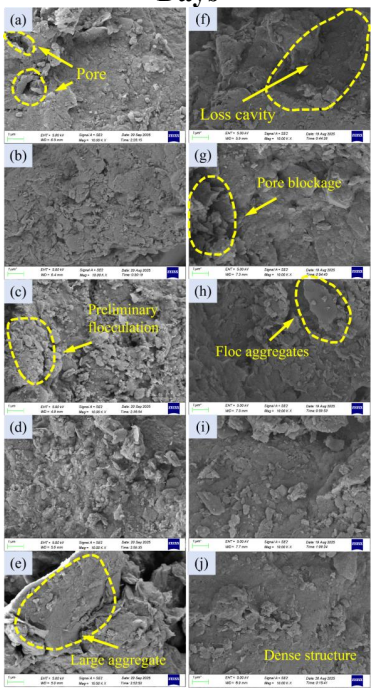

Figure 5. SEM Images of Soil A before and after Permeation. (a, f) Distilled Water; (b, g) 0.3% NaHCO3; (c, h) 1.0% NaHCO3; (d, i) 1.5% NaHCO3; (e, j) 2.0% NaHCO3.

 Copyright @ STEMM Institute Press

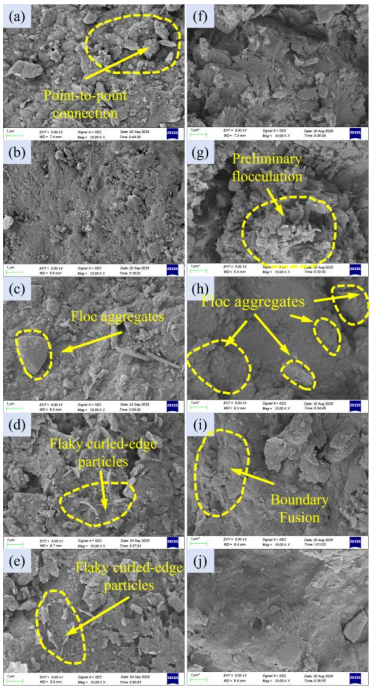

Figure 6. SEM Images of Soil B before and after Permeation. (a, f) Distilled Water; (b, g) 0.3% NaHCO3; (c, h) 1.0% NaHCO3; (d, i) 1.5% NaHCO3; (e, j) 2.0% NaHCO3.

List of Table captions

Table 1–Ion Content and Physical Properties of Naturally Dispersive Soils

Table 2–Mineralogical composition of dispersive soils.

Table 1. Ion Content and Physical Properties of Naturally Dispersive Soils

Contents and properties	SoilA	SoilB
Natural saline soil ion contents (%)		
Anions		
Cl-	0.018	0.053
SO_4^{2-}	0.046	0.023
CO_3^-	0.348	0.285
HCO_3^-	0.187	0.078
Cations		
Na^+	0.186	0.113
Ca^{2+}	0.066	0.04
Mg^{2+}	0.025	0.042
K^+	0.019	0.033
Properties of dispersed clay		
Specific gravity, G_s	2.64	2.65
Initial salt content (%)	11.3	22.8
Atterberg limits for fine grain		
Liquid limit, w_L (%)	38.6	40.6
Plastic limit, w_p (%)	19.2	13.2
Compaction study for fine grain		
Maximum dry density, ρ_{dmax} (g/cm^3)	1.63	1.75
Optimum water content, w_{op} (%)	13.5	12.9

Table 2. Mineralogical Composition of Dispersive Soils.

	SoilA	SoilB
Mineral content (%)		
Quartz	48.4	52.9
Potassium feldspar	8.8	7.4
Plagioclase	24.2	13.5
Calcite	11.6	15.5
Dolomitic	2	5.6
Iron pyrite	/	1.7
Clay minerals	5	3.4
Relative content of clay minerals (%)		
Illite	41	21
Kaolinite	10	7
Chlorite	17	8
Illite/smectite smectite	32	64